NANO · MICRO small
www.small-journal.com

Polydopamine-Capped Bimetallic AuPt Hydrogels Enable Robust Biosensor for Organophosphorus Pesticide Detection

Yu Wu, Lei Jiao, Weiqing Xu, Wenling Gu, Chengzhou Zhu, Dan Du, and Yuehe Lin*

Noble metal hydrogels/aerogels with macroscopic nanoassemblies characterized by ultralow density, profuse continuous porosity, and extremely large surface area have gained abundant interest due to not only their tunable physicochemical properties, but also promising applications in catalysis and sensing. Coupling the increased reaction temperature with dopamine-induced effect, herein, a one-step synthetic approach with accelerated gelation kinetics is reported for the synthesis of polydopamine-capped bimetallic AuPt hydrogels. 3D porous nanowire networks with surface functionalization of polydopamine make them a promising biocompatible microenvironment for immobilizing acetylcholinesterase (AChE) and constructing enzyme-based biosensors for sensitive detection of organophosphorus compounds. Taking advantage of their favorable structure and composition, the optimized product exhibits superior electrochemical activity toward thiocholine produced by AChE-catalyzed hydrolysis of acetylthiocholine. Based on the inhibition of organophosphorus pesticide on the enzymatic activity of AChE, the inhibition mode for the detection of paraoxon-ethyl is established, displaying linear regions over the range of 0.5–1000 ng L^{-1} with a low detection limit of 0.185 ng L^{-1}.

1. Introduction

Hydrogels/aerogels as one of the typical macroscopic nanoassemblies, which are made up of different building blocks at the nanoscale, have received great attention due to their unique physicochemical properties in recent years.[1] Combining with the powerful catalytic properties of noble metal nanomaterials,[2] an increasing number of works regarding the wide applications of hydrogels/aerogels in electrochemical energy storage and conversion,[3] has been reported attributing to their profuse continuous porosity, extremely large surface area, and low density. Recent research efforts in this field have led to the tremendous advances in the rational engineering of noble metal nanostructure from the aspect of size, composition, structure, surface morphology, and configuration.[4] Following the pioneering work on the typical sol–gel synthesis of noble metal hydrogels based on the controlled destabilization of the concentrated nanocrystal sols,[5] an important step forward in synthesizing noble metal-based hydrogels was achieved via one-step in situ reduction of metal precursors.[3c,6] For example, temperature-dependent gelation kinetics was observed and a facile yet efficient method for constructing various bimetallic hydrogel systems (e.g., IrCu, PdCu, and AuPt)[3a,6] with accelerated gelation kinetics at the increased reaction temperature was proposed by our group. Accordingly, the shorter gelation time (<6 h) in water was achieved and their electrocatalytic applications in energy conversion have been extensively investigated. Function-led design of noble metal hydrogels/aerogels and in-depth understanding of structure-performance relationship are expected to expand their applications beyond electrocatalysis and pave the way for more advanced functional nanomaterials.

Organophosphorus compounds have been widely used as efficient pesticides in the agricultural area all over the world for decades.[7] The acute toxicity of organophosphorus pesticides (OPs) is closely associated with their capacity to bind acetylcholinesterase (AChE) and irreversibly inhibit their hydrolyzing activity, triggering the accumulation of the neurotransmitter acetylcholine in the central and peripheral nervous system and finally leading to the death.[8] Consequently, efficient and convenient methods for rapid determination and reliable quantification of OPs are in urgent need. Although traditional analytical methods involving gas chromatography or high-performance liquid chromatography can always provide exact results,[9] they are laborious and associated with the requirement of highly qualified technicians and expensive instruments, consequently limiting their widespread implementation in different fields. Fortunately, the development of nanomaterials has fueled the possibility of designing a branch number of optical and electrochemical sensing platforms for sensitive detection of OPs.[10] Among them, electrochemical AChE-based biosensors featuring the specificity of the enzyme

Y. Wu, L. Jiao, W. Xu, Prof. W. Gu, Prof. C. Zhu
Key Laboratory of Pesticide and Chemical Biology of Ministry of Education
International Joint Research Center for Intelligent Biosensing Technology and Health
College of Chemistry
Central China Normal University
Wuhan 430079, P. R. China
E-mail: czzhu@mail.ccnu.edu.cn
Prof. D. Du, Prof. Y. Lin
School of Mechanical and Materials Engineering
Washington State University
Pullman, WA 99164, USA
The ORCID identification number(s) for the author(s) of this article can be found under https://doi.org/10.1002/smll.201900632.

DOI: 10.1002/smll.201900632

and the high sensitivity of electrochemical transducers have been attracting an extraordinary amount of interest for the sensitive detection of OPs.[11] Constructing the effective matrix that combines enzyme immobilization and excellent electrocatalytic activity toward signal species plays a significant role in fabricating high-performance enzyme-based biosensors for targets.[12] 3D porous noble metal nanostructures with surface functionalization and excellent intrinsic electrocatalytic activity are expected to provide a promising biocompatible microenvironment for immobilizing AChE and construct high-performance enzyme-based biosensors.

Herein, with the assistance of dopamine, polydopamine (PDA)-capped AuPt (AuPt-PDA) hydrogels were successfully synthesized by a one-step method in aqueous solution at the elevated temperature. The gelation kinetics was significantly accelerated and the resultant hydrogels can be obtained within 2 h. Note that the formation time was the shortest among metal hydrogels reported previously. 3D porous nanowire networks with surface functionalization of PDA make AuPt-PDA hydrogels promising biocompatible microenvironment for immobilizing AChE and constructing enzyme-based biosensors for the detection of paraoxon-ethyl (a model compound of OPs) (**Scheme 1**). In addition, good conductivity, accelerated mass transfer as well as the superior catalytic activity toward signal species due to the synergistic effect between compositions enables the AuPt-PDA nanowire networks to achieve electrochemical signal amplification, leading to highly sensitive biosensing for paraoxon-ethyl. Also, this resultant enzyme-inhibited type biosensor was successfully applied to detect the target in pretreated tap and lake water samples, implying a promising application in environmental monitoring.

2. Results and Discussion

AuPt-PDA hydrogels were synthesized based on the former strategy in our group with few improvements. 0.1×10^{-3} mol fresh $NaBH_4$ solution was rapidly injected into 33 mL mix solution containing 10 µmol $HAuCl_4$, 10 µmol H_2PtCl_6, and 2.5 mg dopamine under stirring at 60 °C for 60 s. It was found that metal precursors could be rapidly reduced upon addition of reducing agent, accompanying the color change in the solution. After keeping the solution still for 2 h at 60 °C, black hydrogels precipitated on the bottom of the bottle. The formation process of AuPt-PDA hydrogels was shown in Figure S1 in the Supporting Information. It should be noted that the introduction of dopamine at the increased reaction temperatures further speed up the reaction process and accelerate the gelation kinetics, realizing the evolution of product within 2 h. This formation time is faster than those of counterpart synthesized only at elevated temperature (≈4 h) and other metal hydrogels reported previously (Table S1, Supporting Information).[3c,e,6,13]

In order to study the morphology of AuPt-PDA hydrogels, a supercritical CO_2 drying technique was used to obtain AuPt-PDA aerogels, which was further characterized by scanning electron microscopy (SEM). As shown in **Figure 1**A, the AuPt-PDA aerogels exhibit a porous and nanowire-like nanostructure with large amounts of pores, indicating a promising nanocarrier

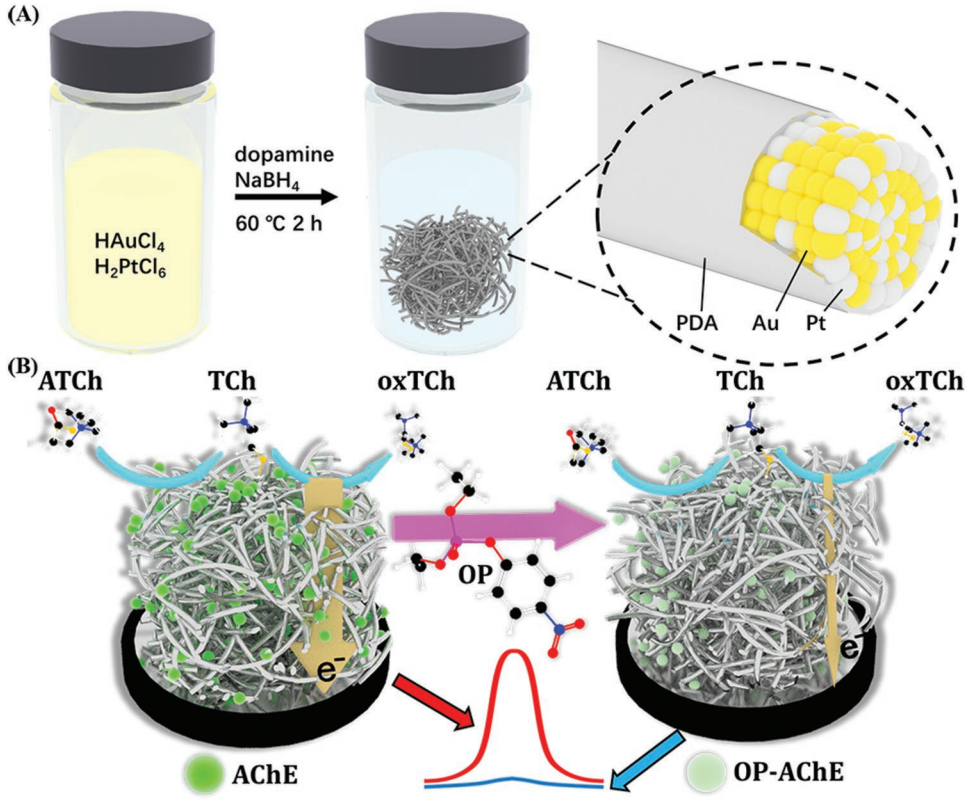

Scheme 1. A) Schematic illustration for the synthesis process of AuPt-PDA hydrogels and B) mechanism of OPs electrochemical detection.

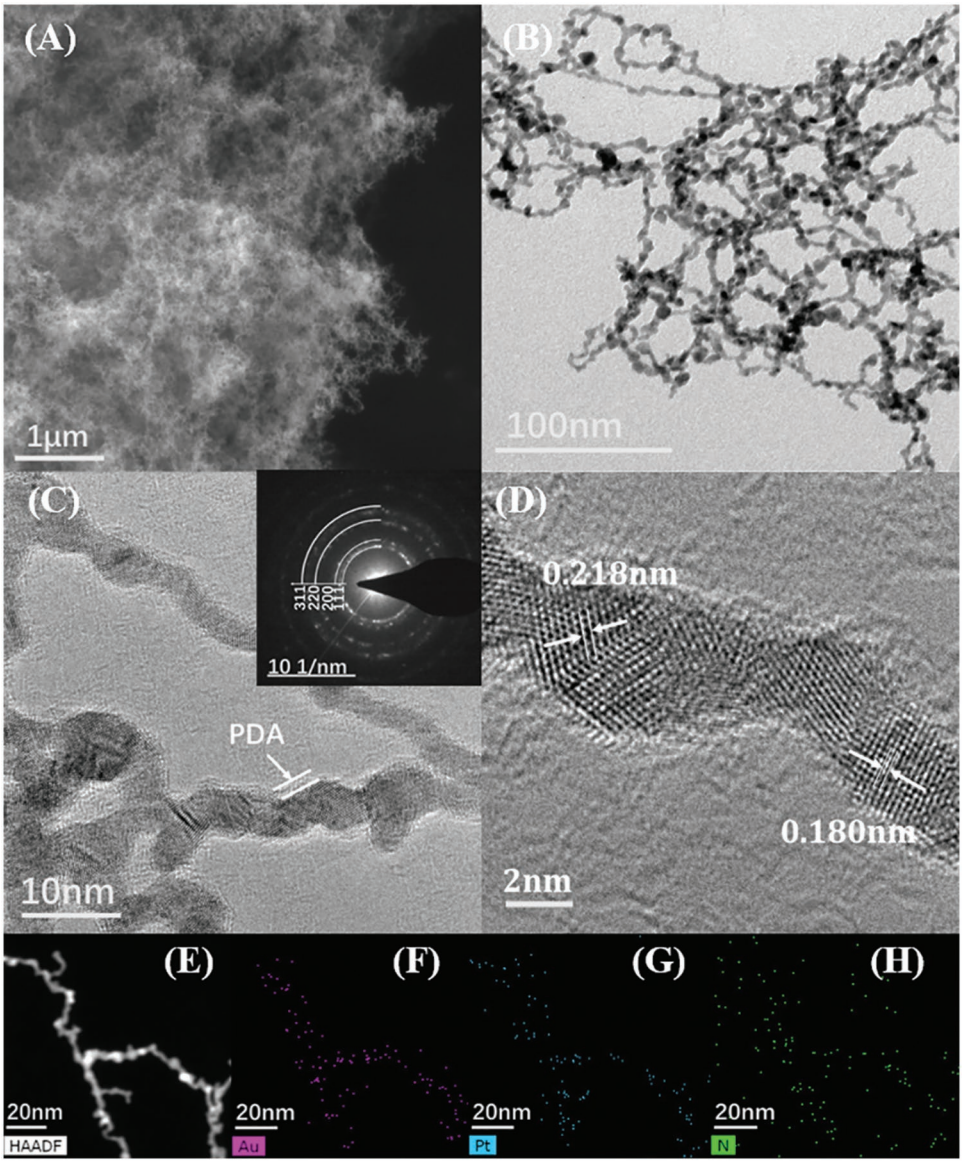

Figure 1. A) SEM image, B,C) TEM image, SAED pattern (inset in (C)), and D) HRTEM image of the resultant AuPt-PDA aerogels. E) HAADF image of AuPt-PDA aerogels and F–H) HAADF mapping images for Au, Pt, and N, respectively.

for loading enzymes. Then, transmission electron microscopy (TEM) was used for further fine structural characterizations. It could be clearly seen from Figure 1B that the as-prepared AuPt-PDA aerogels possess an irregular 3D network structure consisting of interconnected nanowires with an average diameter of 5 nm. Close observation of the structure suggests that these nanowires are coated by one layer of PDA with the thickness of 2 nm, indicating that dopamine plays a significant role in inducing the assembly of the formed nanocrystals (Figure 1C).[6b] The effect of dopamine on the hydrogel formation was investigated and it was found that the introduction of dopamine significantly promotes the gelation process and reduces the hydrogel formation time. However, no obvious change in morphology was found regardless of dopamine, demonstrating that the formation of these hydrogels conforms to the mechanism of oriental attachment (Figure S2, Supporting Information).[14] The selected-area electron diffraction (SAED) pattern (inset in Figure 1C) demonstrated the face-centered cubic (fcc) crystalline of AuPt-PDA aerogels. Furthermore, distances of lattice spacings provided by high-resolution transmission electron microscopy (HRTEM) in Figure 1D are measured as 0.218 and 0.180 nm, corresponding to the (111) facet and the (200) facet of fcc of AuPt-PDA aerogels, respectively. The high-angle annular dark field scanning transmission electron microscopy-energy dispersive spectroscopy (HAADF-STEM-EDS) mapping images in Figure 1E–H confirmed the homogenous distribution of Au and Pt along these nanowires. Not only metal elements, but N element located along nanowires could be obviously observed, manifesting that PDA distributes evenly on the AuPt alloy nanowires.

To validate the fact that PDA was successfully attached to the surface of hydrogels, Fourier transform infrared (FT-IR)

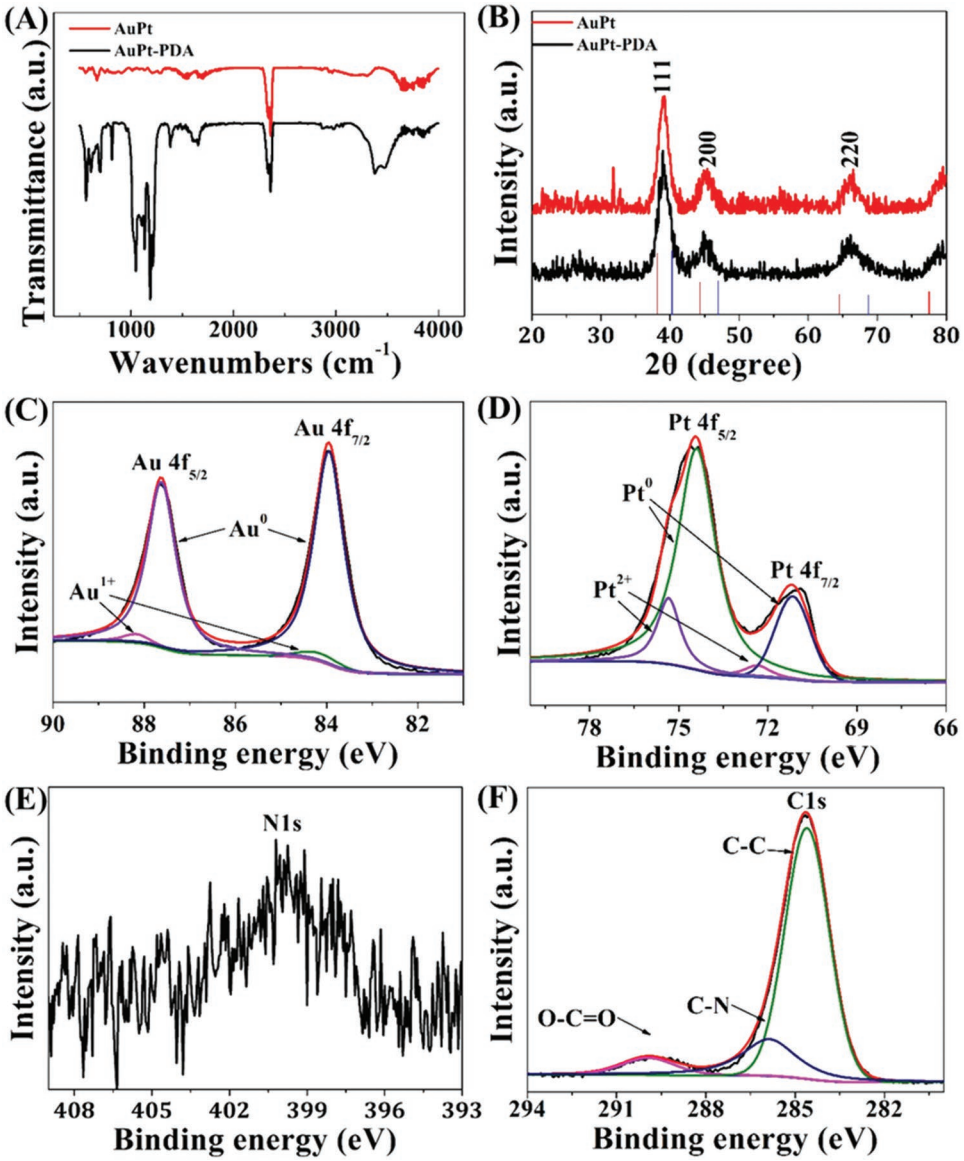

Figure 2. A) FT-IR spectra, B) XRD patterns of AuPt and AuPt-PDA aerogels, XPS spectra of C) Au 4f, D) Pt 4f, E) N 1s, F) C 1s of AuPt-PDA aerogels.

spectrometer was used to characterize both AuPt and AuPt-PDA aerogels. **Figure 2**A shows clear differences between these two samples, peaks at 1515 and 1605 cm^{-1} of the AuPt-PDA aerogels are consistent with indole or indoline structures of PDA.[15] X-ray diffraction (XRD) patterns in Figure 2B demonstrated that no interference was caused by the PDA on the AuPt alloy structure. Besides, three diffraction peaks could be, respectively, assigned to the (111), (200), (220) planes of the fcc crystal structure of the AuPt alloy, according to the fcc Au (PDF#04-0784) and fcc Pt (PDF#04-0802) lattices. X-ray photoelectron spectroscopy (XPS) analysis showed the existence of Au (Figure 2C), Pt (Figure 2D), N (Figure 2E), and C (Figure 2F), which is consistent with the result mentioned above.

One prominent property of noble metal materials is their intrinsically good electrical conductivity and electrocatalytic activity, which has facilitated the establishments of a branch number of electrochemical applications. On the other hand, 3D porous nanowire networks with profuse pores and surface modification of PDA provide an ideal matrix to immobilize enzymes and further construct enzyme-based biosensors toward a variety of targets. Inspired by their attractive structures mentioned above, the resultant AuPt-PDA hydrogels are expected to serve as nanocarriers for AChE immobilization, realizing the inhibition mode for rapid determination of paraoxon-ethyl, a model compound of OPs, simultaneously. In this system, acetylthiocholine (ATCh), a derivate of acetylcholine, can also be hydrolyzed by AChE into thiocholine (TCh), an electroactive compound so that can be detected electrochemically. Therefore, the current intensity from the oxidation of TCh (oxTCh) declined along with the increase of OPs due to their inhibition effect on AChE. Cyclic voltammetry (CV) and electrochemistry impedance spectroscopy (EIS) were first performed to measure the electron transfer ability of AuPt-PDA hydrogels (Figure S3, Supporting Information), both of them were carried

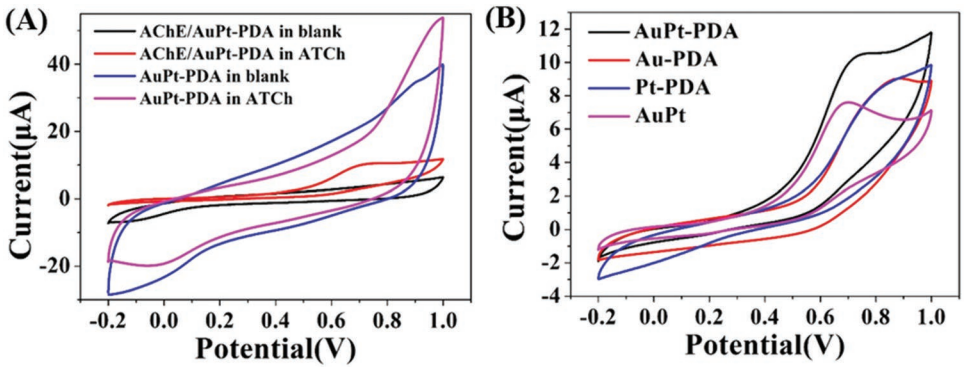

Figure 3. A) CV curves of GCE modified with AuPt-PDA hydrogels and AChE/AuPt-PDA integrations in the absence and presence of 0.2×10^{-3} M ATCh in PBS (0.02 M, pH 7.5). B) CV curves of GCE modified with AChE-loaded AuPt-PDA, Au-PDA, Pt-PDA, and AuPt hydrogels in PBS (0.02 M, pH 7.5) containing 0.2×10^{-3} M ATCh.

out in 0.1 M KCl solution with 5.0×10^{-3} M $K_3[Fe(CN)_6]$. After the modification of AuPt-PDA hydrogels, the peak current of the CV curve obtained at AuPt-PDA hydrogels increased evidently in comparison to bare glassy carbon electrode (GCE), showing an enhanced electron transfer process. This result was also verified by the lower charge-transfer resistance value of AuPt-PDA from EIS patterns. Upon immobilization of AChE, the lower current intensity in the CV curve and larger charge-transfer resistance in EIS were observed, reflecting the successful immobilization of the enzyme. Likewise, the immobilization efficiency of AChE in AuPt-PDA hydrogels was also confirmed by the confocal laser scanning microscope (Figure S4, Supporting Information). Rhodamine B isothiocyanate (RhB) was used as a fluorescent probe to label AChE, and the red fluorescence emission from RhB-labeled AChE in AuPt-PDA hydrogels demonstrated its capability to retain AChE after centrifugation.[16] Then, the electrocatalytic oxidation of TCh was evaluated at AuPt-PDA hydrogels-modified electrode. As shown in **Figure 3**A, with the participation of AChE, AuPt-PDA hydrogels-modified electrode showed an irreversible oxidation peak at 0.65 V, originating from the oxidation of TCh produced by AChE-catalyzed hydrolysis of ATCh, while the hydrolysis and oxidation could not be initiated in the absence of AChE.

The effect of the metal mole ratio on the electrocatalytic performance was also studied and the result was shown in Figure S5 in the Supporting Information. Among these three AuPt-PDA hydrogels, Au_1Pt_1-PDA hydrogels afford the best electrocatalytic performance in terms of high current density and low onset potential. In detail, AuPt-PDA hydrogels are superior to monometallic hydrogels (Figure 3B), showing 1.2-fold catalytic current improvement over both pure Au and Pt. As mentioned above, the introduction of PDA is expected to provide a promising biocompatible microenvironment for immobilizing AChE because of their abundant functional groups.[17] To validate our hypotheses, 5,5'-dithio-bis (2-nitrobenzoic acid), a classical agent for the quantification of thiols,[18] was used to react with TCh. As can be seen from Figure S6 in the Supporting Information, the obtained yellow solution exhibits a distinct peak at 412 nm in the UV-vis spectrum, providing visual results corresponding to different concentrations of generated TCh. In contrast with AuPt hydrogels, AuPt-PDA hydrogels showed higher absorbance, demonstrating their effectiveness for accommodating more AChE. As expected, this unique AChE/AuPt-PDA integration triggers the enhanced electrocatalytic activity and the peak current density was found to increase by a factor of 1.3 for AuPt-PDA hydrogels in comparison with AuPt hydrogels (Figure 3B). Besides, the improved electrochemical response obtained at AuPt-PDA can be ascribed to the following aspects: 1) Zeta-potential of AuPt-PDA hydrogels was measured to be −25.2 mV, indicating a static interaction with positively charged ATCh and TCh. 2) Strong coordination interactions between Au, Pt, and S make AuPt-PDA hydrogels further accelerate the accumulation of the TCh. 3) 1D nanowire structure possesses higher electrocatalytic performances than nanoparticles.[19] 4) AuPt-PDA nanowire networks with increased surface area and facilitated mass transfer are of great significance for their enhanced electrochemical performance.

Upon addition of OPs, AChE lost the hydrolysis ability because of the blocked active sites. Therefore, the detection of paraoxon-ethyl could be established by using electrochemical methods to evaluate the activity of AChE. Based on the optimized parameters (Figure S7, Supporting Information), the OPs biosensor was fabricated by immersing modified electrode into the solution containing different concentrations of paraoxon-ethyl for 15 min, followed by washing carefully with phosphate buffer saline (PBS, 0.02 M, pH 7.5). Differential pulse voltammetry (DPV) was selected as the method to monitor the variation of paraoxon-ethyl concentration from 0.5 to 1000 ng L^{-1}. It could be seen from **Figure 4**A that the oxidation of TCh on AChE/AuPt-PDA caused an obvious oxidation peak at approximate 0.65 V. What is more, the electrochemical response declined with the escalating concentration of paraoxon-ethyl, which was ascribed to the loss of AChE activity. Three parallel experiments by DPV method were carried out to obtain the standard deviation for error bars, and the relationship between inhibition rate and paraoxon-ethyl concentration was described in Figure 4B. Results showed that the current intensity has a linear relationship with the concentration of paraoxon-ethyl in the range from 0.5 to 1000 ng L^{-1} ($1.8–3633.7 \times 10^{-12}$ M), with a low limit of detection (LOD) of 0.185 ng L^{-1} (0.672×10^{-12} M). Besides a wide linear range, our developed biosensor gives an ultralow LOD, which shows an order of magnitude lower than those of former reports (Table S2, Supporting Information).[10b,11a,20]

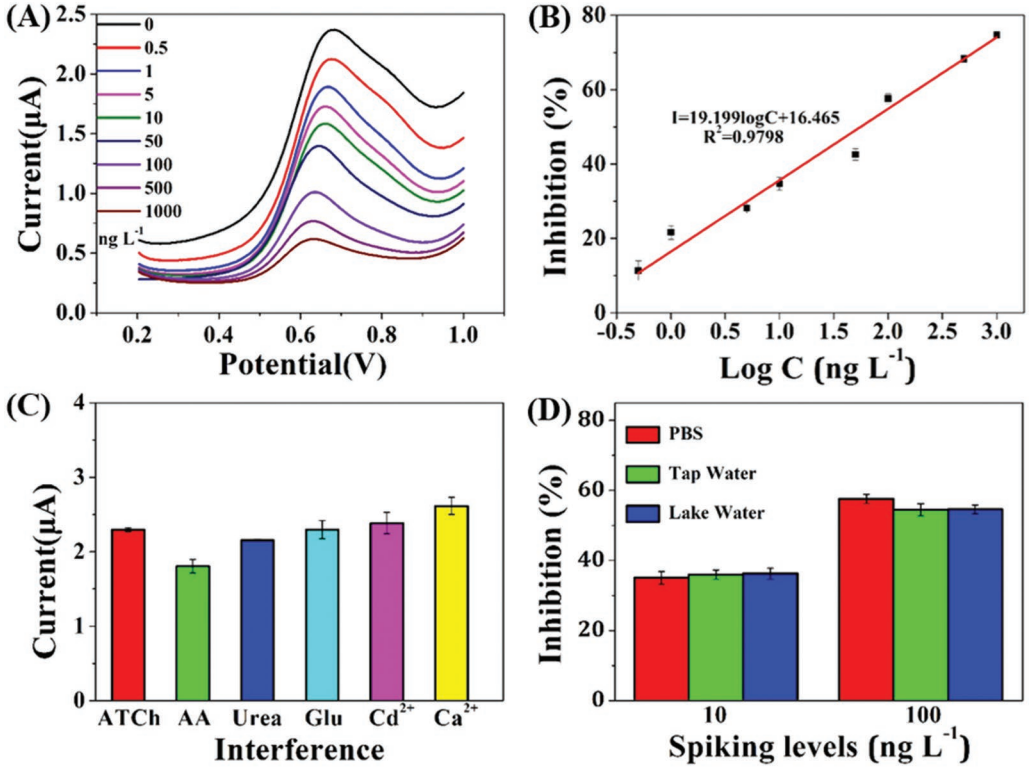

Figure 4. A) DPV responses of the AChE/AuPt-PDA system with different concentration of paraoxon-ethyl (0, 0.5, 1, 5, 10, 50, 100, 500, and 1000 ng L^{-1}). B) Calibration curve of paraoxon-ethyl detection with a range of 0.5–1000 ng L^{-1}. C) Current response of the as-prepared biosensor in PBS (0.02 M, pH 7.5) containing 0.2×10^{-3} M ATCh and interferes (2.0×10^{-3} M). D) Recovery tests performed in tap water and lake water for the detection of paraoxon-ethyl at the spiking level of 10 and 100 ng L^{-1}, respectively.

Some common interfering species were selected to explore the interference resistance of the biosensor. As shown in Figure 4C, the electrochemical response changed negligibly with the presence of urea, glucose, Cd^{2+}, and Ca^{2+}. However, the electrochemical response showed a decline when ascorbic acid was added, which could be explained by the pH change.[11a] For further evaluation of the practical application of the developed biosensor, two recovery tests were performed for tap and lake water (Figure 4D), respectively. Two spiking levels of 10 and 100 ng L^{-1} in the sample were selected. Recovery percentages obtained from tap water were 102.68% and 103.46%, respectively, while 94.63% and 94.86% were obtained from lake water, indicating a great promise to apply this biosensor in environmental and biological monitoring of OPs.

3. Conclusion

In this work, one-step synthetic approach with accelerated gelation kinetics was reported for the synthesis of PDA-capped bimetallic AuPt hydrogels via combining the increased reaction temperature with dopamine-induced effect. We presented here the first electrochemical biosensor based on noble metal hydrogels for the detection of OPs. The obtained AuPt-PDA hydrogels with good biocompatibility, porosity, and high surface area serve as superb platforms to immobilize AChE. Based on the unique structure and excellent electrocatalytic performance, AChE/AuPt-PDA integrations were successfully applied to monitor the concentration of OPs. The proposed biosensor showed a wide linearity range from 0.5 to 1000 ng L^{-1} with a low detection limit (0.185 ng L^{-1}). Therefore, this work based on noble metal hydrogels provides a promising way for enzyme immobilization and OPs analysis.

4. Experimental Section

Synthesis of AuPt-PDA and Other Hydrogels: In a typical synthesis of Au_1Pt_1-PDA hydrogels, 10 μmol $HAuCl_4$ and 10 μmol H_2PtCl_6 were dissolved into 33 mL H_2O containing 2.5 mg dopamine. Two mL 0.05 M fresh prepared $NaBH_4$ solution was quickly injected into the Au, Pt, and dopamine mixture under stirring at 60 °C for about 60 s. Metallic hydrogels could be obtained after 2 h still at 60 °C. Au-PDA, Pt-PDA, and AuPt-PDA with different metal proportions could be obtained by changing the ratio of metal precursors but keeping the total amounts of metal precursors and the amount of dopamine. Besides that, AuPt hydrogels could be prepared through the same method except for the addition of dopamine.

The as-prepared hydrogels were washed with water three times and then dissolved into 10 mL ultrapure water by sonication for the use in next steps.

Preparation of AChE/Hydrogels Integrations: AChE was dissolved into PBS (0.02 M, pH 7.5) to obtain 1 mg mL^{-1} AChE solution. 0.5 mL AChE solution was mixed with 0.5 mL hydrogels solution and then sonicated for 10 s. AChE and hydrogels mixed solution was centrifuged and redispersed to remove the unbinding enzyme. Finally, AChE/hydrogels integrations were obtained by repeating the process three times.

Preparation of Biosensor: Five µL AChE/Au_1Pt_1-PDA integrations were dropped onto the surface of polished GCE and then dried in the air at room temperature. Then 3 µL 0.2% Nafion was placed onto GCE for enhancing the immobilization. The modified electrode was stored at 4 °C before use. GCEs modified with other AChE/hydrogels integrations were prepared by the same method.

Determination of OPs: All the electrochemistry experiments were conducted on a three-electrode system consisting of a GCE as the working electrode, a platinum wire electrode as the counter electrode, and an Ag/AgCl electrode as a reference electrode. Before the analysis of the paraoxon-ethyl, parameters, such as AChE concentration, ATCh concentration, and inhibition time, were further optimized. DPV method was selected to measure the electric signal under the potential from 0.2 to 1.0 V (potential increment: 5 mV, pulse amplitude: 50 mV, pulse width: 50 ms).

The detect mechanism of this biosensor is based on the activity of AChE, so the inhibition rate (I%) can represent a linear relationship with the concentration of paraoxon-ethyl. AChE after inhibition lost the ability to catalyze the oxidation of TCh so that generated a weak current signal (denoted as I_1) comparing with the signal from the uninhibited AChE (denoted as I_0). Therefore, I% can be calculated by the following formula

$$\mathrm{I}(\%) = \frac{I_0 - I_1}{I_0} \times 100 \quad (1)$$

The modified GCEs were immersed into solutions containing different concentrations (0.5, 1, 5, 10, 50, 100, 500, and 1000 ng L^{-1}) of paraoxon-ethyl for 15 min, respectively. Then, the modified GCEs were washed by PBS (0.02 M, pH 7.5) three times to remove unbound paraoxon-ethyl. The DPV analysis was carried out in PBS (0.02 M, pH 7.5) with 0.2×10^{-3} M ATCh.

Real Sample Analysis: Real water samples contained many interferes so that a pretreatment was necessary. Both tap and lake water samples were spiked with paraoxon-ethyl after a filtration. Then the water samples were diluted to 10 and 100 ng L^{-1} with ultrapure water.

Supporting Information

Supporting Information is available from the Wiley Online Library or from the author.

Acknowledgements

The authors gratefully acknowledge the financially supported by the Fundamental Research Funds for the Central Universities (CCNU19QN066), the Program of Introducing Talents of Discipline to Universities of China (111 program, B17019), and The Recruitment Program of Global Youth Experts of China.

Conflict of Interest

The authors declare no conflict of interest.

Keywords

biosensors, electrocatalysis, enzyme immobilization, noble metal hydrogels, organophosphorus pesticides detection

Received: February 2, 2019
Revised: March 14, 2019
Published online:

[1] a) J. L. Mohanan, I. U. Arachchige, S. L. Brock, *Science* **2005**, *307*, 397; b) W. Liu, A.-K. Herrmann, N. C. Bigall, P. Rodriguez, D. Wen, M. Oezaslan, T. J. Schmidt, N. Gaponik, A. Eychmüller, *Acc. Chem. Res.* **2015**, *48*, 154; c) H. Shigemitsu, T. Fujisaku, W. Tanaka, R. Kubota, S. Minami, K. Urayama, I. Hamachi, *Nat. Nanotechnol.* **2018**, *13*, 165.

[2] a) C. Zhu, D. Du, A. Eychmueller, Y. Lin, *Chem. Rev.* **2015**, *115*, 8896; b) L. Bu, N. Zhang, S. Guo, X. Zhang, J. Li, J. Yao, T. Wu, G. Lu, J.-Y. Ma, D. Su, X. Huang, *Science* **2016**, *354*, 1410.

[3] a) Q. Shi, C. Zhu, H. Zhong, D. Su, N. Li, M. H. Engelhard, H. Xia, Q. Zhang, S. Feng, S. P. Beckman, D. Du, Y. Lin, *ACS Energy Lett.* **2018**, *3*, 2038; b) Q. Shi, C. Zhu, M. Tian, D. Su, M. Fu, M. H. Engelhard, I. Chowdhury, S. Feng, D. Du, Y. Lin, *Nano Energy* **2018**, *53*, 206; c) W. Liu, P. Rodriguez, L. Borchardt, A. Foelske, J. Yuan, A.-K. Herrmann, D. Geiger, Z. Zheng, S. Kaskel, N. Gaponik, R. Kötz, T. J. Schmidt, A. Eychmüller, *Angew. Chem., Int. Ed.* **2013**, *52*, 9849; d) B. Cai, A. Dianat, R. Hübner, W. Liu, D. Wen, A. Benad, L. Sonntag, T. Gemming, G. Cuniberti, A. Eychmüller, *Adv. Mater.* **2017**, *29*, 1605254; e) D. Wen, W. Liu, D. Haubold, C. Zhu, M. Oschatz, M. Holzschuh, A. Wolf, F. Simon, S. Kaskel, A. Eychmueller, *ACS Nano* **2016**, *10*, 2559.

[4] a) B. Cai, A. Eychmüller, *Adv. Mater.* **2018**, https://doi.org/10.1002/adma.201804881; b) Q. Shi, C. Zhu, Y. Li, H. Xia, M. H. Engelhard, S. Fu, D. Du, Y. Lin, *Chem. Mater.* **2016**, *28*, 7928.

[5] N. C. Bigall, A.-K. Herrmann, M. Vogel, M. Rose, P. Simon, W. Carrillo-Cabrera, D. Dorfs, S. Kaskel, N. Gaponik, A. Eychmüller, *Angew. Chem., Int. Ed.* **2009**, *48*, 9731.

[6] a) C. Zhu, Q. Shi, S. Fu, J. Song, H. Xia, D. Du, Y. Lin, *Adv. Mater.* **2016**, *28*, 8779; b) Q. Shi, C. Zhu, D. Du, C. Bi, H. Xia, S. Feng, M. H. Engelhard, Y. Lin, *J. Mater. Chem. A* **2017**, *5*, 19626.

[7] G. Mercey, T. Verdelet, J. Renou, M. Kliachyna, R. Baati, F. Nachon, L. Jean, P.-Y. Renard, *Acc. Chem. Res.* **2012**, *45*, 756.

[8] a) Y. Miao, N. He, J.-J. Zhu, *Chem. Rev.* **2010**, *110*, 5216; b) D. M. Quinn, *Chem. Rev.* **1987**, *87*, 955.

[9] a) S. Mahpishanian, H. Sereshti, *J. Chromatogr. A* **2016**, *1443*, 43; b) J. I. Cacho, N. Campillo, P. Viñas, M. Hernández-Córdoba, *J. Chromatogr. A* **2018**, *1559*, 95.

[10] a) W. Zhang, A. M. Asiri, D. Liu, D. Du, Y. Lin, *TrAC, Trends Anal. Chem.* **2014**, *54*, 1; b) X. Yan, Y. Song, C. Zhu, H. Li, D. Du, X. Su, Y. Lin, *Anal. Chem.* **2018**, *90*, 2618; c) M. Liang, K. Fan, Y. Pan, H. Jiang, F. Wang, D. Yang, D. Lu, J. Feng, J. Zhao, L. Yang, X. Yan, *Anal. Chem.* **2013**, *85*, 308; d) H. Ouyang, X. Tu, Z. Fu, W. Wang, S. Fu, C. Zhu, D. Du, Y. Lin, *Biosens. Bioelectron.* **2018**, *106*, 43; e) J. F. Chang, H. Y. Li, T. Hou, F. Li, *Biosens. Bioelectron.* **2016**, *86*, 971.

[11] a) F. Zhao, Y. Yao, X. Li, L. Lan, C. Jiang, J. Ping, *Anal. Chem.* **2018**, *90*, 11658; b) H. Cui, W. Wu, M. Li, X. Song, Y. Lv, T. Zhang, *Biosens. Bioelectron.* **2018**, *99*, 223; c) C. Zhu, G. Yang, H. Li, D. Du, Y. Lin, *Anal. Chem.* **2015**, *87*, 230.

[12] a) D. Zhai, B. Liu, Y. Shi, L. Pan, Y. Wang, W. Li, R. Zhang, G. Yu, *ACS Nano* **2013**, *7*, 3540; b) Q. Wang, X. Zhang, L. Huang, Z. Zhang, S. Dong, *Angew. Chem., Int. Ed.* **2017**, *56*, 16082; c) F. Zhao, J. Wu, Y. Ying, Y. She, J. Wang, J. Ping, *TrAC, Trends Anal. Chem.* **2018**, *106*, 62.

[13] a) C. Zhu, Q. Shi, S. Fu, J. Song, D. Du, D. Su, M. H. Engelhard, Y. Lin, *J. Mater. Chem. A* **2018**, *6*, 7517; b) W. Liu, A.-K. Herrmann, D. Geiger, L. Borchardt, F. Simon, S. Kaskel, N. Gaponik, A. Eychmüller, *Angew. Chem., Int. Ed.* **2012**, *51*, 5743.

[14] a) Z. Peng, H. You, H. Yang, *ACS Nano* **2010**, *4*, 1501; b) W. Hong, C. Shang, J. Wang, E. Wang, *Energy Environ. Sci.* **2015**, *8*, 2910; c) H.-G. Liao, L. Cui, S. Whitelam, H. Zheng, *Science* **2012**, *336*, 1011.

[15] D. R. Dreyer, D. J. Miller, B. D. Freeman, D. R. Paul, C. W. Bielawski, *Langmuir* **2012**, *28*, 6428.

[16] X. Wu, J. Ge, C. Yang, M. Hou, Z. Liu, *Chem. Commun.* **2015**, *51*, 13408.
[17] H. Lee, J. Rho, P. B. Messersmith, *Adv. Mater.* **2009**, *21*, 431.
[18] X. Chen, Y. Zhou, X. Peng, J. Yoon, *Chem. Soc. Rev.* **2010**, *39*, 2120.
[19] a) H.-H. Li, S. Zhao, M. Gong, C.-H. Cui, D. He, H.-W. Liang, L. Wu, S.-H. Yu, *Angew. Chem., Int. Ed.* **2013**, *52*, 7472; b) D. Wen, S. Guo, S. Dong, E. Wang, *Biosens. Bioelectron.* **2010**, *26*, 1056.
[20] a) G. Yu, W. Wu, Q. Zhao, X. Wei, Q. Lu, *Biosens. Bioelectron.* **2015**, *68*, 288; b) H. Li, Y. Xu, G. Lu, X. Su, *Sens. Actuators, B* **2018**, *260*, 563; c) L. F. Sgobbi, S. A. S. Machado, *Biosens. Bioelectron.* **2018**, *100*, 290.